Int. J. Heat Mass Transfer. Vol. 35, No. 8, pp. 1977–1985, 1992
Printed in Great Britain

0017–9310/92 $5.00+0.00

Calculation of wall–mass transfer rates in separated aqueous flow using a low Reynolds number k–ε model

S. NEŠIĆ and J. POSTLETHWAITE
Department of Chemical Engineering, University of Saskatchewan, Saskatoon, SK, Canada S7N 0W0

and

D. J. BERGSTROM
Department of Mechanical Engineering, University of Saskatchewan, Saskatoon, SK, Canada S7N 0W0

(*Received* 3 *January* 1991 *and in final form* 25 *July* 1991)

Abstract—Mass transfer in aqueous, turbulent flow through a sudden pipe expansion is simulated with a low Reynolds number (LRN) k–ε eddy viscosity model. The predicted wall–mass transfer rates are tested against experimental data, obtained with electrochemical measurements ($Re = 2.1$–13×10^4 and $Sc = 1460$). LRN modifications to the turbulence model in the near-wall regions, coupled with the turbulent Schmidt number concept, enable successful predictions of wall–mass transfer rates to be obtained. For the specific case of a high Schmidt number fluid, the mass transfer boundary layer is much thinner than the hydrodynamic boundary layer. Furthermore, even low levels of turbulence in the near-wall region are shown to have significant influence on the overall wall–mass transport.

1. INTRODUCTION

IN PRACTICE it is often found that corrosion in aqueous solutions is mass transfer controlled [1, 2]. However, mass transfer in complex flow geometries is strongly influenced by the local hydrodynamic conditions. In a recent erosion–corrosion study [3, 4], the effect of separated flow on mass transfer rates in aqueous solutions was studied by analysing the experimental mass transfer measurements of Sydberger and Lotz [5]. Measured wall–mass transfer rates were correlated with the turbulence levels predicted with a k–ε eddy viscosity model (EVM) for flow through a sudden expansion. The correlation obtained from this set of experimental results, was then successfully used [3] to predict the measured corrosion rates of Lotz and Postlethwaite [6] for a similar flow geometry. Although the specific results obtained so far appear encouraging, there was some concern regarding the generality of the hydrodynamic model. The implementation of the k–ε turbulence model at the wall used the wall function (WF) approach which is strictly incorrect for separated or recirculating flows.

In an attempt to obtain a more general model for prediction of wall–mass transfer rates in separated flow, the hydrodynamic code was revised to include a low Reynolds number (LRN) k–ε model. Unlike the WF approach, a LRN closure attempts to model the turbulent transport across the entire near-wall region. This is especially important for predicting mass transfer at the wall. In the present paper the LRN k–ε model is used to predict wall–mass transfer rates downstream of a sudden expansion in an aqueous flow system. Unlike the previous research noted above, particle transport was not included; instead the study focused on mass transfer in single-phase flow.

In the past two decades, flow through a sudden expansion has been the subject of extensive experimental and numerical investigation, primarily because it represents a generic flow configuration for separation and the associated recirculation, which in turn have a significant effect on a large number of heat and mass transfer devices and processes. One of the first numerical studies was the work of Gosman *et al.* [7], in which they presented predictions for flow through an axisymmetric sudden expansion using a k–ε model. They compared their results against the experimental findings of Back and Roschke [8], and reported good agreement for the reattachment length. Recently, Gould *et al.* [9] compared the results of predictions made with a k–ε model with their own simultaneous two-component LDA measurements in the incompressible turbulent air flow field following an axisymmetrical expansion. They found good agreement for the mean axial velocity, turbulent kinetic energy, and turbulent shear stresses, but poor agreement for the normal turbulent stresses. In an extensive related study, Yap [10] evaluated the performance of several turbulence models for near-wall flow by computing momentum and heat transfer in several recirculating and impinging flows. In particular, the author used both a k–ε EVM and an algebraic stress model (ASM)

NOMENCLATURE

$C_\mu, C_{\varepsilon 1}, C_{\varepsilon 2}$ constants in the k–ε model of turbulence
E constant in the universal velocity profile
f_μ, f_1, f_2 constants in the LRN turbulence model
k kinetic energy of turbulence, $\frac{1}{2}\overline{u_i u_i}$
m species mass concentration
P pressure
P_k production of turbulence
Pr Prandtl number
r radial coordinate
Re Reynolds number
Re_y turbulence Reynolds number, $(\rho y\sqrt{k})/\mu$
Re_T turbulence Reynolds number, $(\rho k^2)/\mu\varepsilon$
S source term
Sc Schmidt number
u, v components of the fluctuation velocity vector
U, V components of mean velocity vector
x axial coordinate
y distance from the wall
y^+ nondimensional distance from the wall.

Greek symbols
Γ diffusion coefficient
ε dissipation of kinetic energy of turbulence, $2\mu/\rho\overline{s_{ij}s_{ij}}$
μ dynamic viscosity
μ_t turbulent viscosity, $C_\mu f_\mu(\rho k^2)/\varepsilon$
ρ fluid, density
$\sigma_\Phi, \sigma_k, \sigma_\varepsilon, \sigma_m$ turbulent Prandtl–Schmidt numbers
Φ general variable.

Subscripts
eff effective value (molecular + turbulent)
k kinetic energy of turbulence
t turbulent value.

to predict the hydrodynamics and heat transfer for flow downstream of a sudden axisymmetric expansion. Near the walls, he considered the use of wall functions, a low Reynolds number model, and a one equation model of turbulence, the latter two being employed with a fine near-wall grid. The best agreement between predictions and experiments for hydrodynamic and heat transfer data was obtained with an ASM/LRN model [11]. Initially the predicted heat transfer rates were 5 times higher than those measured; this led to the use of an extra source term in the dissipation equation, which resulted in significantly improved results.

A number of detailed experimental (LDA) studies of flow through a sudden expansion have recently been published, [12–15], which appear to have resolved the problem of measurements in the near-wall region. However, very few have been conducted with a liquid flow medium. The experimental advantage of using air is one obvious reason. For modelling purposes liquid flows introduce additional complications, since their high Prandtl–Schmidt numbers prevent equating the heat or mass transfer boundary layers with the hydrodynamic boundary layer. Furthermore, the body of published work is directed either towards studying purely hydrodynamic aspects of the flow or determining the effect of the hydrodynamics on heat transfer. Mass transfer studies, such as the numerical study on mixing of helium in turbulent swirling flow in a pipe (Hirai *et al.* [16]) and the experimental investigation of Sydberger and Lotz on the effect of separated aqueous flow on mass transfer in pipes, are rare. The present study is one of the first to consider the application of a LRN model to predict wall–mass transfer in a separated flow.

2. THE MODEL

2.1. *Origin*

In the present study, mass transfer in water flow through a sudden expansion was modelled by a control volume method. The turbulence model is based on the standard k–ε EVM model of Launder and Spalding (TEACH) [17]. The mass transfer is modelled by simultaneously solving a full mass transport equation, with the flow equations and by assuming an analogy in the mechanisms of turbulent momentum and mass transport, via the turbulent Schmidt number concept.

A solution is sought for a set of elliptical partial differential transport equations that all have the same form (in cylindrical coordinates)

$$\frac{\partial}{\partial x}(\rho U\Phi)+\frac{1}{r}\frac{\partial}{\partial r}(r\rho V\Phi)=\frac{\partial}{\partial x}\left(\Gamma_\Phi\frac{\partial\Phi}{\partial x}\right)+\frac{1}{r}\frac{\partial}{\partial r}\left(r\Gamma_\Phi\frac{\partial\Phi}{\partial r}\right)+S_\Phi \quad (1)$$

where $\Phi = U, V, k, \varepsilon, m, \ldots$.

The governing equations for flow and mass transfer are represented in Table 1.

The effective viscosity μ_{eff} and diffusivity D_{eff} are the sum of the molecular and turbulent contributions

$$\mu_{\text{eff}} = \mu+\mu_t$$

$$\underbrace{D_{\text{eff}}}_{\text{effective}} = \underbrace{\frac{\mu}{\rho Sc}}_{\text{molecular}} + \underbrace{\frac{\mu_t}{\rho\sigma_m}}_{\text{turbulent}}.$$

Table 1. Conservation equations

Conservation of	Φ	Γ_Φ	S_Φ
Mass	1	0	0
Axial momentum	U	μ_{eff}	$\frac{\partial}{\partial x}\left(\mu_{\text{eff}}\frac{\partial U}{\partial x}\right)+\frac{1}{r}\frac{\partial}{\partial r}\left(r\mu_{\text{eff}}\frac{\partial V}{\partial x}\right)-\frac{\partial P}{\partial x}$
Radial momentum	V	μ_{eff}	$\frac{\partial}{\partial x}\left(\mu_{\text{eff}}\frac{\partial U}{\partial r}\right)+\frac{1}{r}\frac{\partial}{\partial r}\left(r\mu_{\text{eff}}\frac{\partial V}{\partial x}\right)-2\mu_{\text{eff}}\frac{V}{r^2}-\frac{\partial P}{\partial r}$
Turbulent kinetic energy	k	$\frac{\mu_{\text{eff}}}{\sigma_k}$	$P_k-\rho\varepsilon$
Turbulent dissipation rate	ε	$\frac{\mu_{\text{eff}}}{\sigma_\varepsilon}$	$\frac{\varepsilon}{k}(C_{\varepsilon 1}f_1P_k-C_{\varepsilon 2}f_2\rho\varepsilon)$
Species	m	ρD_{eff}	0

$$P_k=\mu_{\text{eff}}\left\{2\left[\left(\frac{\partial U}{\partial x}\right)^2+\left(\frac{\partial V}{\partial r}\right)^2+\left(\frac{V}{r}\right)^2\right]+\left(\frac{\partial U}{\partial r}+\frac{\partial V}{\partial x}\right)^2\right\}.$$

Following ref. [18] we used a set of well established constants

$$C_\mu=0.09,\quad C_{\varepsilon 1}=1.44,\quad C_{\varepsilon 2}=1.92$$
$$\sigma_k=1.0,\qquad \sigma_\varepsilon=1.3,\qquad \sigma_m=0.9.$$

The value of the turbulent Prandtl–Schmidt number $\sigma_m=0.9$, which is of special importance in mass transfer studies, is, according to Kays and Crawford [19], constant throughout the bulk of the fluid, especially for fluids with high molecular *Pr–Sc* numbers. Measurements have indicated that very close to the wall (in the viscous sublayer) the value of σ_m approximately doubles, however, the exact variation remains to be definitively determined.

2.2. *Boundary conditions*

Since the set of partial differential flow equations (1) is elliptic, it is necessary to define boundary conditions for all variables on all boundaries of the flow domain: inlet, exit, walls and symmetry axis. At the inlet, the mean and fluctuating velocity can be taken from measurements, while zero gradients can be set at the axis and the outlet. Near the wall two basic approaches have been widely used: universal wall functions (WF) model and low Reynolds number (LRN) models (e.g. Jones and Launder [20]).

The WF approach, although the less demanding of the two, from the aspects of required memory and CPU time, is known to perform worse than the LRN approach for recirculating flows [10]. The 'universal' velocity profile determined for simple near-wall shear flows, which is employed in the WF approach, is inappropriate when separation or flow reversal are present. More importantly, for aqueous flows where the Schmidt numbers are of the order of 1000, one can expect that the thickness of the mass transfer diffusion controlled boundary sublayer is an order of magnitude smaller than the thickness of the hydrodynamic viscous sublayer [21]. Thus the WF approach, which bridges over the viscous sublayer with a universal velocity profile, misses important features of the mass transfer boundary layer deeply embedded within it. Instead, a turbulence model is required which can penetrate deep into the hydrodynamic boundary layer, at the same time accounting for the changes in the turbulence structure due to the wall. This suggests that a LRN approach, which enables the extension of the k–ε turbulence model all the way to the wall, should be used in the case of modelling mass transfer in aqueous flow.

Patel *et al.* [22] have made a comparative test of seven different low Reynolds number models. Only three models emerged as 'successful' when tested against experimental data for flows dominated by proximity to the wall. One model was that of Lam and Bremhorst [23] and this has been adopted in the present study. From a physical point of view it is more appealing than the other two recommended models, since it operates with the dissipation rate ε itself rather than with a 'dissipation variable' selected for the sake of computational convenience. More recently, other studies, e.g. ref. [24], have proposed improved LRN models. These models are essentially similar to that of Lam and Bremhorst except for the specific choice of the 'damping functions' f_μ, f_1 and f_2. The model of Lam and Bremhorst was selected for this study, since it contains the essential features of a successful LRN model and has been used in a number of other studies.

In the model of Lam and Bremhorst, the damping functions, which are responsible for the modification of the turbulence field in the near-wall region, are given by

$$f_\mu=[1-\exp(-0.0165Re_y)]^2\left(1+\frac{20.5}{Re_T}\right)$$

Table 2. Important geometric, hydrodynamic and numerical parameters

Outlet Reynolds number	21 000	42 000	84 000	130 000
Inlet diameter [mm]	20	20	20	20
Outlet diameter [mm]	40	40	40	40
Length [mm]	400	400	400	400
Inlet velocity [m s^{-1}]	1.71	3.38	6.75	10.45
Outlet velocity [m s^{-1}]	0.42	0.84	1.68	2.62
Number of x grid-points	80	81	83	86
Number of y grid-points	26	28	29	30
Last grid-point wall distance [μm]	5	3	2	1
Number of iterations	757	870	863	1146
VAX 6320 CPU time [min]	62	82	89	117
Total error of prediction [%]	0.1	0.1	0.1	0.1

$$f_1 = 1+\left(\frac{0.05}{f_\mu}\right)^3$$

$$f_2 = 1-\exp(-Re_T^2) \qquad (2)$$

where

$$Re_y = \frac{\rho y\sqrt{k}}{\mu} \quad \text{and} \quad Re_T = \frac{\rho k^2}{\mu\varepsilon}.$$

At the wall the boundary conditions used for k and ε are

$$k = 0, \quad \frac{\partial\varepsilon}{\partial r} = 0.$$

2.3. *Numerical procedure*

The conservation equations for mass, axial and radial momentum, species, kinetic energy of turbulence and its dissipation rate, are solved numerically using the SIMPLE algorithm, by Patankar and Spalding [25]. The numerical parameters, as well as the geometrical and hydrodynamical parameters of the flows simulated, are given in Table 2.

The criterion for convergence was that the total normalised residual be less than 10^{-3}. Convergence of the solution algorithm was stable, except for the finest grids tested (near-wall node spacing $\leqslant 1$ μm), when the damping functions (2) caused instabilities which resulted in very slow convergence or even divergence. A remedy was found by activating the damping functions only after reasonable convergence (residual $\leqslant 5\times$the convergence criterion) was reached without them. This proved to be very efficient and caused the otherwise divergent solutions to converge using the finest grids, and accelerated the convergence of the algorithm for coarser grids. Physically, this is equivalent to ignoring the influence of walls on turbulence, until we get a 'reasonably' converged solution for the mean flow. This reasonably converged solution was very close to the final solution, as far as the mean flow pattern is concerned, since the flow being simulated is not entirely dominated by wall effects. Thus after activating the damping functions, modification of the flow parameters occurred only in the vicinity of the wall, which did not cause instabilities in the overall solution.

For purely hydrodynamic LRN models it is usually adequate to place the first node adjacent to the wall somewhere in the viscous sublayer ($y^+ < 5$), typically $y^+ \approx 1$. However, in the case of mass transfer at high Schmidt numbers ($Sc \approx 1000$), the thickness of the diffusion mass transfer boundary layer is approximately one tenth of the viscous sublayer. Therefore, the first node was placed at $y^+ \approx 0.1$. The final solution fields have shown that only at these distances from the wall does the level of turbulent transport of mass become negligible compared to the molecular diffusional component.

3. RESULTS AND DISCUSSION

The experimental study of Sydberger and Lotz [5] on the effect of separated, turbulent, aqueous flow on wall–mass transfer rates, was numerically simulated. They used electrochemical measurements to determine wall–mass transfer rates for a system with a Schmidt number of 1460. Among the variety of geometries investigated, we have selected the sudden pipe expansion flow geometry and obtained predictions for four different Reynolds numbers, in the range of 2.1–13×10^4, for which measurements were available. In the paper, the authors omitted reporting specific measurements on most of the figures and instead presented only the best-fit lines. This is unfor-

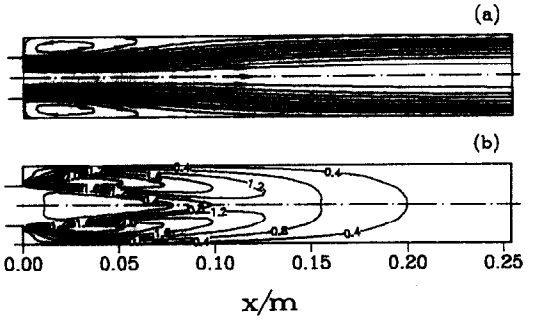

FIG. 1. Predictions for (a) the flow streamlines and (b) corresponding turbulence kinetic energy field. Water flow through a sudden pipe expansion; $d_{in} = 20.0$ mm; $d_{out} = 40.0$ mm; $v_{in} = 1.71$ m s^{-1}; $v_{out} = 0.42$ m s^{-1}; $Re_{out} = 2.1\times10^4$.

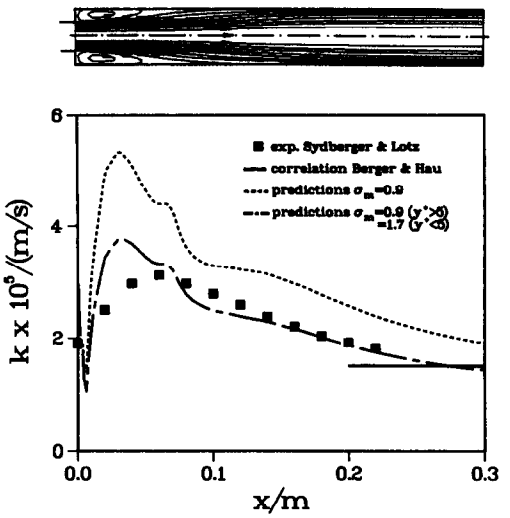

FIG. 2. Predicted flow streamlines and measurements and predictions for the mass transfer coefficients. Water flow through a sudden pipe expansion; $d_{in} = 20.0$ mm; $d_{out} = 40.0$ mm; $v_{in} = 1.71$ m s^{-1}; $v_{out} = 0.42$ m s^{-1}; $Re_{out} = 2.1 \times 10^4$.

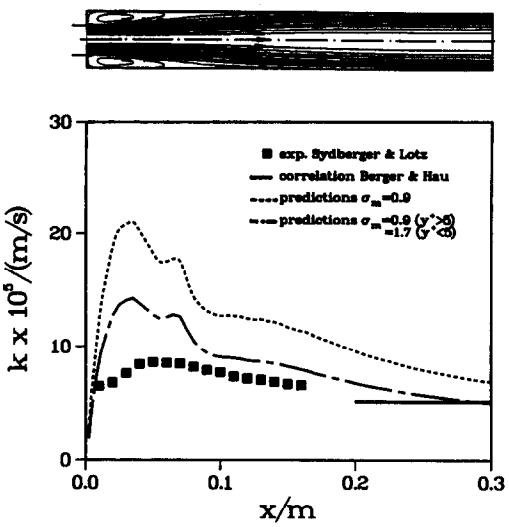

FIG. 4. Predicted flow streamlines and measurements and predictions for the mass transfer coefficients. Water flow through a sudden pipe expansion; $d_{in} = 20.0$ mm; $d_{out} = 40.0$ mm; $v_{in} = 6.75$ m s^{-1}; $v_{out} = 1.68$ m s^{-1}; $Re_{out} = 8.4 \times 10^4$.

tunate as some subtle features of the measured curves, which were not associated with measurement errors, were lost. For example, there are clear indications that the second (smaller) local maximum in the mass transfer coefficient curve, obtained in our predictions (Figs. 2–5), was also present in the measurements. Unfortunately, the local maximum was smoothed out by the best-fit curve.

Predictions for the flow streamlines and the corresponding turbulence kinetic energy field, are shown in Fig. 1 for the Reynolds number $Re = 2.1 \times 10^4$. From the turbulence kinetic energy field (Fig. 1(b)), the major source of turbulence can be clearly identified downstream of the expansion in the bulk flow at the point of maximum shear. The turbulence thus created is transported by convection and reaches the proximity of the wall, creating a local maximum in near-wall turbulence in the region near the reattachment point.

Measured and predicted wall–mass transfer rates expressed in terms of the local mass transfer coefficient are compared in Figs. 2–5, for four different Reynolds numbers. The local values of the mass transfer coefficients were computed on the basis of the predicted local wall–mass flux and the overall concentration difference between the bulk solution and the wall. The

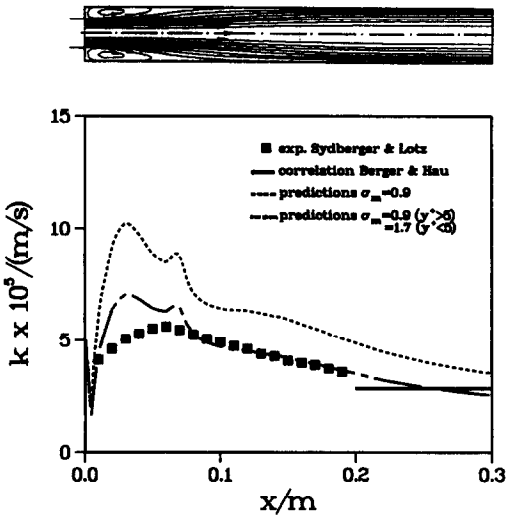

FIG. 3. Predicted flow streamlines and measurements and predictions for the mass transfer coefficients. Water flow through a sudden pipe expansion; $d_{in} = 20.0$ mm; $d_{out} = 40.0$ mm; $v_{in} = 3.38$ m s^{-1}; $v_{out} = 0.84$ m s^{-1}; $Re_{out} = 4.2 \times 10^4$.

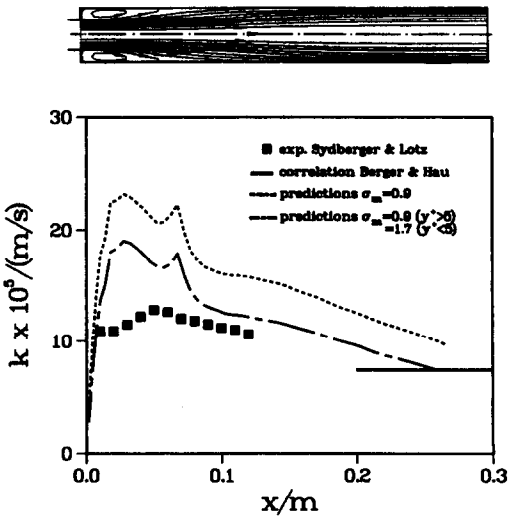

FIG. 5. Predicted flow streamlines and measurements and predictions for the mass transfer coefficients. Water flow through a sudden pipe expansion; $d_{in} = 20.0$ mm; $d_{out} = 40.0$ mm; $v_{in} = 10.45$ m s^{-1}; $v_{out} = 2.62$ m s^{-1}; $Re_{out} = 13.0 \times 10^4$.

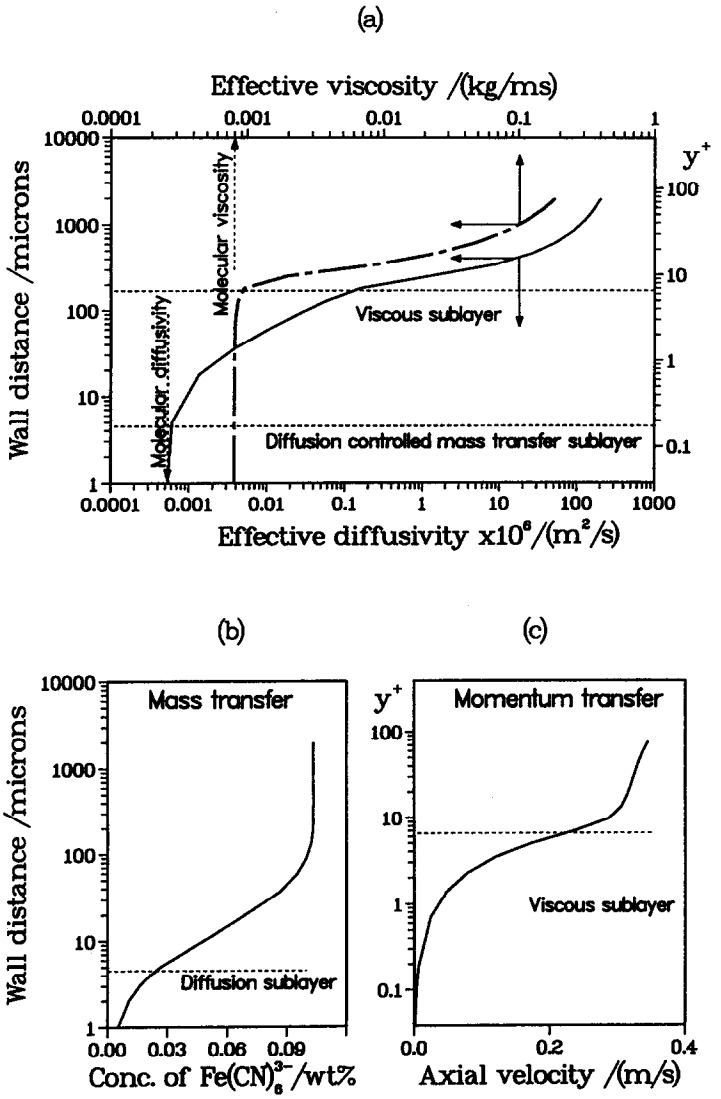

FIG. 6. (a) Transport coefficients, (b) concentration and (c) axial velocity vs wall distance. Water flow through a sudden pipe expansion. Location: redeveloped flow downstream of the reattachment point. $d_{in} = 20.0$ mm; $d_{out} = 40.0$ mm; $v_{in} = 1.71$ m s^{-1}; $v_{out} = 0.42$ m s^{-1}; $Re_{out} = 2.1 \times 10^4$.

predicted profiles follow the shape of the measured curves. The discrepancy is largest for the highest Reynolds numbers, where the smallest effect of the additional turbulence created by the separated flow conditions is expected, because of already high levels of near-wall turbulence. Furthermore, the predictions are closer to the measured values in the region after the reattachment. This can be explained by the fact that the model of turbulence adopted is not strictly valid in the recirculation zone of the flow. Both the measured and predicted profiles far downstream, asymptotically approach the value obtained from the widely accepted straight pipe correlation of Berger and Hau [26]. When the higher value of the turbulent Schmidt number was used in the predictions for the viscous sublayer, $\sigma_m = 1.7$ [19], the maximum discrepancy between the measured and predicted values in the region after the reattachment was reduced from 80% to 10%, while the discrepancy for the maximum mass transfer coefficient was reduced from 120% to 50%. The maximum wall–mass transfer rates occur close to the reattachment point and coincide with the local maximum in turbulent momentum and mass transport. The location of the predicted maximum was upstream from the measured values, which can be attributed to the overprediction of turbulent transport in the recirculation zone.

Turbulent transport overrides the diffusional transport of mass in the bulk flow by several orders of magnitude. It is only very close to the wall in the viscous sublayer, where the turbulent transport is damped, that the two mechanisms have comparable effects. This can be seen in Figs. 6 and 7 which show the predicted momentum and mass transfer transport

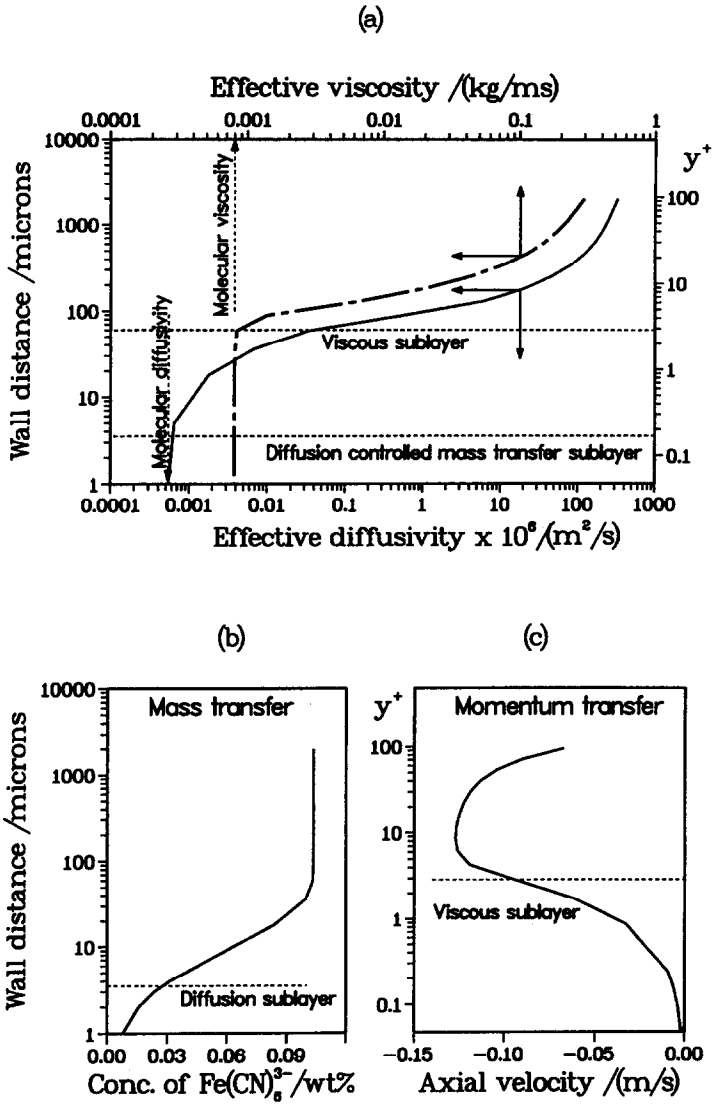

FIG. 7. (a) Transport coefficients, (b) concentration and (c) axial velocity vs wall distance. Water flow through a sudden pipe expansion. Location: recirculation region upstream of the reattachment point. $d_{in} = 20.0$ mm; $d_{out} = 40.0$ mm; $v_{in} = 1.71$ m s^{-1}; $v_{out} = 0.42$ m s^{-1}; $Re_{out} = 2.1 \times 10^4$.

coefficients μ_{eff} and D_{eff}, and the corresponding variables U and m, in the near wall region for $Re = 2.1 \times 10^4$, at two locations: in the redeveloped flow region and just before the reattachment.

The transport coefficients (Figs. 6(a) and 7(a)) are shown on a log–log scale, because of the large range involved. Figure 6 shows predictions downstream of the expansion where fully redeveloped turbulent flow can be assumed. Figure 6(a) shows that far away from the wall ($y \geqslant 1$ mm) the value of the effective viscosity is 100 times larger than the molecular value; thus the flow is dominated by turbulent transport. As we approach closer to the wall ($y \approx 200$ μm) the magnitude of the effective viscosity approaches the value of the molecular viscosity, indicating that the turbulence is gradually being damped. Consequently a line can be drawn ($y \approx 150$ μm) that denotes the edge of the viscous sublayer, in which region the flow is controlled by viscous forces. In terms of the standard wall coordinates, this is very close to $y^+ = 5$ as expected [27]. The predicted axial velocity profile on a semi-log scale is shown in Fig. 6(c). The profile has the well-known universal shape: linear in the viscous sublayer and logarithmic in the law-of-the-wall region.

Similar conclusions may be reached for mass transfer. The effective diffusivity in the bulk flow is 5 orders of magnitude higher than molecular diffusivity (Fig. 6(a)), indicating that turbulent mixing is very intense. Concentration profiles obtained for the bulk are flat; changes are only noticed when the viscous sublayer is approached (Fig. 6(b)). In the outer part of the viscous sublayer the turbulent viscosity is less than 1% of the effective viscosity, indicating that very little

turbulence is retained. Nevertheless, the effective diffusivity is still 100 times larger than the molecular diffusivity. This suggests that the residual turbulence, which is not significant from the momentum transport point of view, is very significant from the mass transfer point of view. This behaviour is to be expected for fluids with large Schmidt numbers. Turbulent mass transport is reduced as the wall is approached, becoming insignificant some 5 μm from the wall ($y^+ \approx 0.2$) when mass is transported exclusively by molecular diffusion. The thickness of the molecular diffusion controlled mass transfer sublayer $\delta_m \approx 5$ μm, compared to the thickness of the viscous sublayer $\delta \approx 150$ μm, is very close to the ratio suggested by Levich [21], i.e. $\delta_m = \delta/Sc^{0.33}$. The predicted concentration profile, which in analogous fashion to the velocity profile exhibits the linear and logarithmic portions is shown in Fig. 6(b). Note that both regions are embedded in the viscous sublayer of the momentum boundary layer.

Figure 7 contains similar information to Fig. 6, for the region of the wall just before the reattachment point. Due to the increased turbulence in this region, both the hydrodynamic and mass transfer boundary layers are thinner, but still retain a similar ratio. The velocity profile, in the region above the viscous sublayer reflects the flow reversal associated with the recirculation.

4. CONCLUSIONS

Mass transfer in aqueous, turbulent, recirculating flow was simulated with a LRN k–ε EVM model. The predictions were tested against experimental data [5] for flow through a sudden pipe expansion ($Re = 2.1$–13×10^4 and $Sc = 1460$). Good agreement was obtained over the whole range, without any 'tuning' of the transport equations or turbulence model.

For flows with high Schmidt numbers, the mass transfer boundary layer is completely embedded within the viscous sublayer. Low levels of turbulent transport in the viscous sublayer, insignificant from the hydrodynamic point of view, override the diffusional mass transport throughout most of the hydrodynamic viscous sublayer. Thus, the diffusion controlled mass transfer sublayer is much thinner than the viscous sublayer. Although not initially intended for application in the viscous sublayer, modifications to turbulence models for near-wall regions, coupled with the use of the turbulent Schmidt number, enable successful predictions of mass transfer rates in complex turbulent recirculating flow even for high Schmidt numbers.

Acknowledgement—The support of this research by the Natural Sciences and Engineering Research Council of Canada is gratefully acknowledged.

REFERENCES

1. J. Postlethwaite, M. H. Dobbin and K. Bergevin, The role of oxygen mass transfer in the erosion–corrosion of slurry pipelines, *Corrosion* **42**, 514–521 (1986).
2. B. K. Mahato, S. K. Voora and L. W. Shemilt, Steel pipe corrosion under flow conditions—I. An isothermal correlation for a mass transfer model, *Corros. Sci.* **8**, 173–193 (1968).
3. S. Nešić and J. Postlethwaite, Hydrodynamics of disturbed flow and erosion–corrosion, Part I—a single-phase flow study, *Can. J. Chem. Engng* **69**, 698–703 (1990).
4. S. Nešić and J. Postlethwaite, Hydrodynamics of disturbed flow and erosion–corrosion, Part II—a two-phase flow study, *Can. J. Chem. Engng* **69**, 704–710 (1990).
5. T. Sydberger and U. Lotz, Relation between mass transfer and corrosion in a turbulent pipe flow, *J. Electrochem. Soc.* **129**, 276–283 (1982).
6. U. Lotz and J. Postlethwaite, Erosion–corrosion in disturbed two phase liquid/particle flow, *Corros. Sci.* **30**, 95–106 (1990).
7. A. D. Gosman, E. E. Khalil and J. H. H. Whitelaw, The calculation of two-dimensional turbulent recirculating flow. In *Turbulent Shear Flows I* (Edited by F. Durst, B. E. Launder, F. W. Schmidt and J. H. Whitelaw), pp. 237–255. Springer, New York (1979).
8. L. H. Back and E. J. Roschke, Shear-layer flow regimes and wave instabilities and reattachment lengths downstream of an abrupt circular channel expansion, *ASME J. Appl. Mech.* **94**, 677–681 (1972).
9. R. D. Gould, W. H. Stevenson and H. D. Thompson, Investigation of turbulent transport in an axisymmetric sudden expansion, *AIAA J.* **28**, 276–283 (1990).
10. C. R. Yap, Turbulent heat and momentum transfer in recirculating and impinging flows, Ph.D. Thesis, University of Manchester, Manchester, U.K. (1987).
11. J. W. Baughn, M. A. Hoffman, B. E. Launder, D. Lee and C. Yap, Heat transfer, temperature and velocity measurements downstream of an abrupt expansion in a circular tube at a uniform wall temperature, *ASME J. Heat Transfer* **111**, 870–876 (1989).
12. L. Khezzar, J. H. Whitelaw and M. Yianneskis, An experimental study of round sudden expansion flows, *Proc. 5th Symp. Turb. Shear Flows*, Cornell University, pp. 5–25 (1985).
13. R. T. Szczepura, Flow characteristics of an axisymmetric sudden pipe expansion: results obtained from the turbulence studies rig, Part 1: mean and turbulence velocity results, Report TPRD/0702/N85, CEGB, Berkeley Nuclear Laboratories, U.K. (1985).
14. R. P. Durret, W. H. Stevenson and H. D. Thompson, Radial and axial turbulent flow measurements with an LDV in an axisymmetric sudden expansion air flow, *ASME J. Fluids Engng* **110**, 367–372 (1988).
15. M. Stieglmeier, C. Tropea, N. Weiser and W. Nitsche, Experimental investigation of the flow through axisymmetric expansions, *ASME J. Fluids Engng* **111**, 464–471 (1989).
16. S. Hirai, T. Takagi and T. Higashiya, Numerical prediction of flow characteristics and retardation of mixing in a turbulent swirling flow, *Int. J. Heat Mass Transfer* **32**, 121–130 (1989).
17. B. E. Launder and D. B. Spalding, The numerical computation of turbulent flows, *Comp. Meth. Appl. Mech. Engng* **3**, 269–289 (1974).
18. D. Milojević, T. Borner and F. Durst, Prediction of turbulent gas–particle flow measurement in a plain confined jet, World Congress Particle Technology, Part IV, Partikel Technologie Nurnberg, Nurnberg, W. Germany (1986).
19. W. M. Kays and M. E. Crawford, *Convective Heat and Mass Transfer*, pp. 225–229. McGraw-Hill, New York (1980).
20. W. P. Jones and B. E. Launder, The calculation of low-Reynolds number phenomena with a two-equation model of turbulence, *Int. J. Heat Mass Transfer* **16**, 1119–1130 (1973).

21. V. Levich, *Physicochemical Hydrodynamics*, pp. 144–154. Prentice-Hall, Englewood Cliffs, NJ (1962).
22. V. C. Patel, W. Rodi and G. Scheurer, Turbulence models for near-wall and low Reynolds number flows: a review, *AIAA J.* **23,** 1308–1319 (1985).
23. C. K. G. Lam and K. Bremhorst, A modified form of the k–ε model for predicting wall turbulence, *ASME J. Fluids Engng* **103,** 456–460 (1981).
24. Y. Nagano and M. Hishida, Improved form of the k–ε model for wall turbulent shear flows, *ASME J. Fluids Engng* **109,** 156–160 (1987).
25. S. V. Patankar and D. B. Spalding, A calculation procedure for heat, mass and momentum transfer in three-dimensional parabolic flows, *Int. J. Heat Mass Transfer* **15,** 1787–1806 (1972).
26. F. P. Berger and K.-F, F.-L. Hau, Mass transfer in turbulent pipe flow measured by the electrochemical method, *Int. J. Heat Mass Transfer* **20,** 1185–1194 (1977).
27. H. Tennekes and J. L. Lumley, *A First Course in Turbulence*, pp. 156–162. MIT Press, Cambridge, MA (1987).

CALCUL DES FLUX PARIETAUX DE MASSE DANS UN ECOULEMENT D'EAU, A L'AIDE D'UN MODELE k–ε A FAIBLE NOMBRE DE REYNOLDS

Résumé—Le transfert de masse dans un écoulement turbulent d'eau à travers un élargissement brusque est simulé par un modèle à viscosité turbulente k–ε à faible nombre de Reynolds. Les flux de masse calculés sont testés avec les données expérimentales obtenues par des mesures électrochimiques ($Re = 2{,}1$–13×10^4 et $Sc = 1460$). Les modifications LRN du modèle de turbulence dans les régions proches de la paroi, couplées avec le concept de nombre de Schmidt turbulent, donnent des prédictions correctes des flux de masse obtenus. Pour le cas particulier d'un fluide à nombre de Schmidt élevé, la couche limite de transfert de masse est plus mince que la couche hydrodynamique. Par conséquent, même des niveaux faibles de turbulence dans la région proche de la paroi ont une influence sensible sur le transfert pariétal de masse.

BERECHNUNG DES STOFFTRANSPORTS IN EINER ABGELÖSTEN WÄSSRIGEN STRÖMUNG MIT HILFE EINES k–ε-MODELLS FUR KLEINE REYNOLDS-ZAHLEN

Zusammenfassung—Es wird der Stofftransport in einer wäßrigen turbulenten Strömung durch eine plötzliche Rohrerweiterung mit einem k–ε-Modell für die Wirbelviskosität bei kleiner Reynolds-Zahl simuliert. Der berechnete Stofftransport an der Wand wird mit Hilfe von Versuchsdaten überprüft, die mit elektrochemischen Messungen gewonnen worden sind ($Re = 2{,}1$–13×10^4 und $Sc = 1460$). Durch LRN-Modifikationen am Turbulenzmodell in den wandnahen Bereichen, gekoppelt mit dem Konzept der turbulenten Schmidt-Zahl, kann der zu erwartende Stofftransport erfolgreich vorausberechnet werden. Für den Spezialfall eines Fluids mit großer Schmidt-Zahl ist die Grenzschichtdicke für den Stofftransport sehr viel kleiner als die hydrodynamische Grenzschichtdicke. Weiterhin wird gezeigt, daß sogar eine nur geringfügige Turbulenz im wandnahen Gebiet den gesamten Stofftransport signifikant beeinflußt.

ОПРЕДЕЛЕНИЕ СКОРОСТЕЙ МАССОПЕРЕНОСА НА СТЕНКЕ ПРИ СОРВАННОМ ПОТОКЕ ВОДЫ С ИСПОЛЬЗОВАНИЕМ k–ε МОДЕЛИ ПРИ НИЗКИХ ЧИСЛАХ РЕЙНОЛЬДСА

Аннотация—С использованием k–ε модели турбулентной вязкости с низкими числами Рейнольдса описывается массоперенос при турбулентном течении воды во внезапно расширяющемся участке трубы. Рассчитанные скорости массопереноса от стенки сравниваются с экспериментальными данными, полученными с помощью электрохимических измерений ($Re = 2{,}1$–13×10^4 и $Sc = 1460$). Модификации модели с низкими числами Рейнольдса применительно к турбулентности в пристенных областях в комбинации с концепцией турбулентного числа Шмидта позволяют удовлетворительно определить скорости массопереноса на стенке. В случае большого числа Шмидта для жидкости тепловой пограничный слой массопереноса намного тоньше гидродинамического. Показано, что даже низкие уровни турбулентности в пристенной области оказывают существенное влияние на результирующий массоперенос на стенке.